Hierarchical Arrangement of P(VDF-TrFE) Copolymer Crystals: A SAXS and AFM Study

Pedro Resende, Sara Zanchi, Jean-David Isasa, Raymond Khayat, Georges Hadziioannou, Guillaume Fleury

Hierarchical Arrangement of P(VDF-TrFE) Copolymer Crystals: A SAXS and AFM Study

Pedro M. Resende, Sara Zanchi, Jean-David Isasa, Raymond Khayat, Georges Hadziioannou, Guillaume Fleury**

Univ. Bordeaux, CNRS, Bordeaux INP, LCPO, UMR 5629, F-33600, Pessac, France

Corresponding Authors: *pdecamposres@u-bordeaux.fr*, *gfleury@enscbp.fr*

Keywords: SAXS, AFM, P(VDF-TrFE), Morphology.

Abstract

P(VDF-TrFE) copolymers are materials with high relevance in printed organic electronics. These copolymers easily crystallize into the ferroelectric phase without resorting to post-deposition treatments (thermal annealing, poling, or mechanical stretching). The detection of a morphotropic phase boundary further increased the interest in this copolymer system by demonstrating relaxor behavior for higher TrFE content. This prompted an in-depth analysis of the P(VDF-TrFE) chiral chain structure responsible for the relaxor properties. Nevertheless, the efficient application of these materials also depends heavily on the quality and morphology of the crystalline domains. In this work, we combine SAXS and AFM imaging to analyze the structure of the crystalline domains as a function of the TrFE content. The detection of different structural distributions revealed the presence of hierarchical arrangements within the crystalline domains. Furthermore, these hierarchical arrangements were observed to change with the TrFE monomer content, presenting distinct morphologies for low and high TrFE contents, in line with previous works on the morphotropic phase boundary in these systems.

Introduction

In the field of printed organic electronics, poly(vinylidene fluoride-*co*-trifluoroethylene) [P(VDF-TrFE)] copolymer thin films have garnered significant attention, largely due to their outstanding ferroelectric,

piezoelectric, and pyroelectric properties.[1–4] The electroactivity of these semi-crystalline fluorinated polymers is attributed to the strong overall dipolar moment along the *b*-axis of the polymer chains. The inclusion of TrFE units in these copolymers promotes the formation of all-*trans* conformations along the polymer backbone, leading to ferroelectric behavior without the need for additional post-treatments. Increasing amounts of TrFE result in increasing *gauche* conformational defects and in chirality-induced relaxor ferroelectric properties associated with the expansion of the crystalline lattice parameters.[5–7] While all-*trans* conformations result in a dense ferroelectric (FE) crystalline phase, the increase in *gauche* conformations leads to the formation of defective crystalline phases depending on the TrFE content. In the literature, these phases are referred as defective ferroelectric (DFE) and relaxor ferroelectric (RFE) phases. DFE phases are distinct from RFE phases in that they contain fewer *gauche* defects, have smaller lattice parameters, and possess the ability to be polarized under an external electric field.[8] A similar expansion of the lattice parameters due to the inclusion of *gauche* defects has also been observed on the copolymerization of VDF and TFE (tetrafluoroethylene) monomers. Above a critical TFE content a *gauche* defect containing phase exists for P(VDF-TFE) copolymers characterized by larger lattice parameters compared to the all-*trans* phase.[9]

The arrangement of dipoles in the FE, DFE, or RFE crystalline phases of P(VDF-TrFE) copolymers plays a pivotal role in determining their electroactive properties. Consequently, extensive research has been conducted to understand how chemical composition and processing conditions influence the crystalline structure and, thus, the electroactive behavior of these polymers.[5,10–14,7,15,16] In 1989, Tashiro and Kobayashi published a seminal structural study of P(VDF-TrFE) copolymers based on X-ray diffraction and infrared and Raman spectroscopy.[10] Their work led to the establishment of a phase diagram of the existing crystalline phases as a function of copolymer composition and temperature. In addition to the VDF/TrFE ratio, processing conditions also have a crucial effect on the crystalline phases. The standard process to produce P(VDF-TrFE) thin films, used in organic electronics, is solvent-casting. After the evaporation of the solvent, which may occur at room temperature or require higher temperatures, an annealing step in the paraelectric phase is commonly employed to increase the crystallinity and attain more homogeneous and better electroactive properties.[5,14] Regardless of the chemical composition or the thermal treatment, only a limited number of studies have thoroughly explored the effects of processing conditions on the morphology of P(VDF-TrFE) films. These studies have

primarily resorted to characterization techniques such as Scanning Electron Microscopy (SEM),[4,17,18] Atomic Force Microscopy (AFM),[19–24] and Small Angle X-ray Scattering (SAXS).[8,24–26] Microscopy images showed that after annealing the morphology is characterized by small rice-like grains, homogeneous in size and shape, whose size changes with the annealing temperature. SAXS analyses have mainly showed a shift towards smaller angles with increasing temperatures, interpreted as an increase of the long period (L_p), which is irreversible after the thermal treatment. By performing PeakForce AFM analyses, Hafner *et al.* recently observed that these rice-like domains are made of alternating crystalline lamellae and amorphous layers.[22] Thermal treatments above the melting temperature of P(VDF-TrFE) thin films are known to give rise to a very different morphology, consisting in very extended and thick needle-like crystalline structures. In this case, the crystalline lamellae show a preferential orientation, namely parallel (flat-on) or perpendicular (edge-on) to the substrate.[20,24] The orientation of the crystalline domains with respect to the substrate has a strong effect on the electric responsiveness of the film. Edge-on stacks give the strongest response, since they are characterized by dipolar moments whose rotation planes are parallel to the crystalline lamellae and thus to an external electric field. Flat-on stacks are undesirable, because the dipolar moments are perpendicular to the electric field and consequently not affected by it. The intermediate tilted orientation give rise to an intermediate behavior.[15,27]

The available literature regarding the effect of the chemical composition on the morphology of P(VDF-TrFE) copolymers is notably limited, since most of the reported research is usually focused on a restricted set of compositions (one or two samples) and do not explore the possible impact of this parameter. For example, Hirose *et al.* showed the evolution of the long period and the lamellar and amorphous thicknesses with respect to the temperature, for samples containing 73% and 52% VDF. However, they did not provide an in-depth discussion of the differences observed between these compositions.[25] Similarly, Jiang *et al.* reported SEM images of the morphology of three different samples (70%, 55% and 50% VDF), yet their analysis did not extend to a comprehensive discussion of the morphological differences.[18]

It is important to note that when SAXS and microscopy analyses are taken individually it becomes challenging to give a complete and clear understanding of the morphology of P(VDF-TrFE) copolymer films. Coupled

SAXS-AFM studies are known to be a powerful tool, for instance, to study the self-assembly of block copolymers and colloidal systems. Despite this, almost none of the existing studies has focused on fluorinated polymers. A recent study combined SAXS and AFM results for a P(VDF-TrFE) copolymer and four P(VDF-TrFE-CTFE) terpolymers to understand the evolution of their morphology with respect to the CTFE (chlorotrifluoroethylene) content and with respect to the thermal treatment (below or above the melting temperature).[24] Independently from the thermal treatment, the authors measured a slight increase of the long period with the CTFE content, so with the increase of *gauche* conformational defects. Moreover, the SAXS patterns showed the existence of at least two contributions: one at higher *q* values, associated with the long period (around 15 nm), and at least one at lower *q*, associated with the parallel stacking of some lamellae. These results were consistent with their AFM observations, showing the interest of such coupled studies for fluorinated polymers.

In this article, we present a comprehensive study on the morphology of P(VDF-TrFE) copolymers, employing a combination of SAXS and AFM for different P(VDF-TrFE) samples. To conduct this analysis, we prepared samples by drop-casting polymer solutions, followed by a gentle thermal treatment to ensure the gradual evaporation of the solvent, without disturbing the arrangement of the polymer chains and avoiding structural quenching. Six chemical compositions were explored, ranging from 20 mol.% to 79 mol.% of TrFE, to understand the role of TrFE in determining the morphology of P(VDF-TrFE) films. The dual SAXS-AFM analysis allows the proper identification of the different structural features, serving as valuable tools to understand morphological evolutions in polymeric systems.

Materials and Methods

Materials: The P(VDF-TrFE) copolymers employed in this work were kindly supplied by Piezotech (Arkema). According to the manufacturer, the six different copolymers have a TrFE molar content of 20%, 25%, 30%, 50%, 57%, and 79%. Copolymer compositions were also independently confirmed with NMR. Additional information on copolymer molecular weight and dispersity (obtained from SEC combined with the refractive

index increment dn/dc) is provided in the Supporting Information (SI). Triethyl phosphate (TEP) used as casting solvent was purchased from Sigma-Aldrich.

Polymer Thin Film: Thin films were prepared through solution drop-casting. Solutions of 15 wt.% were prepared in TEP (room temperature, stirred for 48 h). Previously cleaned glass substrates were used for the deposition. The polymer solutions and the substrates were kept under the same temperature conditions, thermalized to room temperature. The polymer solutions were poured onto the substrates and allowed to spread and relax across the surface (less than 1 min). After, the as-cast films were dried at 90 °C, for 2 h 20 min, on a hot plate, and under atmospheric pressure. The low solvent evaporation due to its high boiling point resulted in a slow drying process, this allows the polymer to relax and resulted in uniform and isotropic films. No shearing forces were applied during film deposition. The prepared thin films were detached from the glass substrates by wetting with deionized water, separating the films without damage.

Electron Microscopy: SEM imaging was performed with a JEOL 7800-E PRIME (Jeol Ltd., Japan), under low current (< 50 pA) and low voltage (< 1 kV) settings. A conductive coating of 2 nm of platinum was deposited with a magnetron sputtering system (Leica EM ACE600), decreasing charge accumulation. The ImageJ open-source software was used for micrograph analysis.

Small Angle X-ray Scattering: SAXS data were recorded with a WAXS/SAXS system (Xeuss 2.0 from XENOCS), under vacuum and ambient temperature. The sample-to-detector distance was 2480 mm with a beam size of 0.25 mm², and λ = 1.54 Å (Cu Kα). The scattered radiation was collected with a Dectris Pilatus-300k detector, for a q range of *ca.* 0.004 to 0.17 $Å^{-1}$, and azimuthally integrated. Data analysis was made with Origin. Additional information on data analysis is provided in the SI.

AFM: AFM imaging was performed with a Dimension FastScan® equipment (Bruker) in PeakForce Quantitative Nanomechanics (QNM) mode. ScanAsyst-Fluid+ probes (nominal frequency: 150 kHz; nominal spring constant: 0.7 N/m; nominal tip radius: 2 nm) were used. The scan rate and lines were set at 0.5 Hz and 1024, respectively, to increase the resolution of the scans. Topography and adhesion images were analyzed to characterize the surface morphology of the samples.

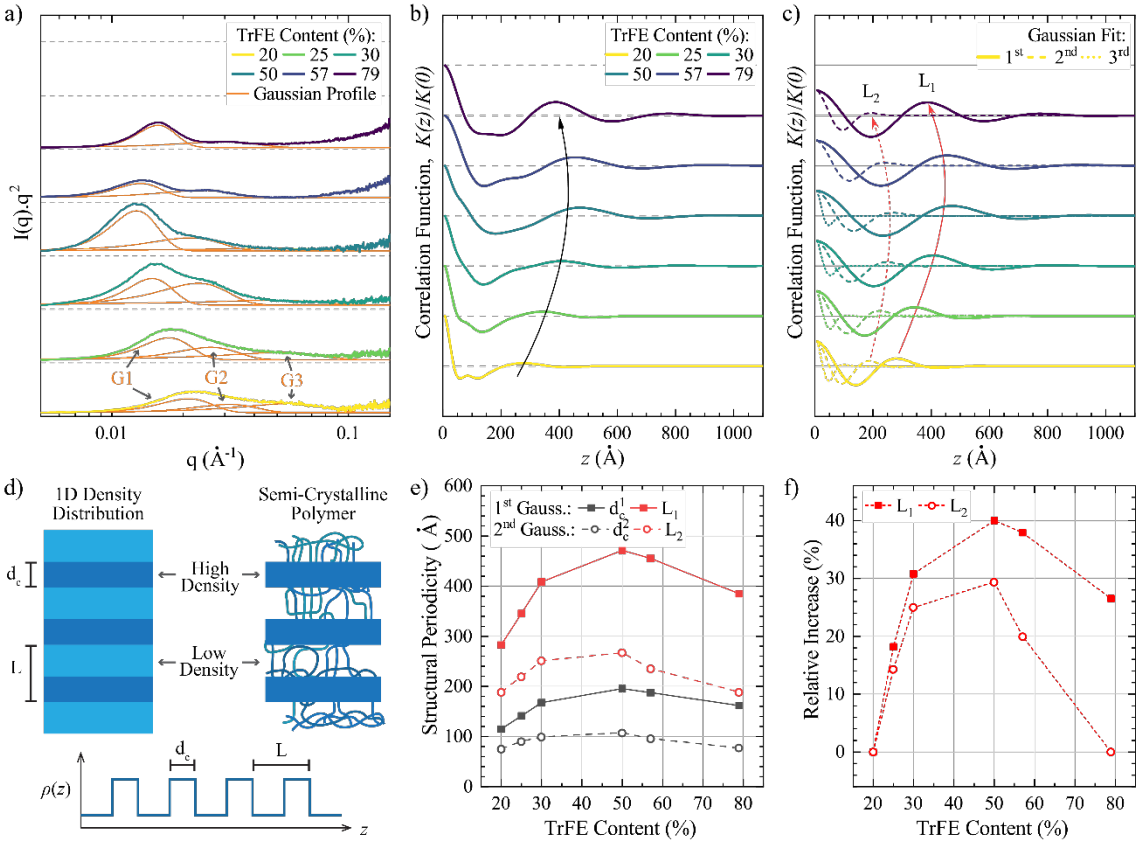

Figure 1. SAXS profiles and corresponding correlation functions. a) Lorentz corrected SAXS profiles for the different produced films, along with the fitted Gaussian profiles (labelled G1 to G3), showing a gradual shift of the distributions with TrFE content. b) Calculated correlation functions from the extrapolated cumulative fits of the SAXS diffractograms. c) Calculated correlation functions for the individual Gaussian profiles (G1 to G3) for each TrFE composition. The position of the first maxima corresponds to the long period L (L_1 for G1 profiles, and L_2 for G2 profiles) of each distribution, shifting with sample TrFE content. d) Scheme of the layered/lamellar structure in semi-crystalline polymers and material density distribution. e) Long-period, L, and size of the crystalline domains, d_c, extracted from the individual correlation functions of the first two Gaussian (G1 and G2) profiles. The longest structural periodicities are obtained for 50% TrFE. f) Relative increase in the long period size (L_1 and L_2), normalized to 20% TrFE. The maxima are observed for 50% TrFE, with L_2 returning to its initial value for 79% TrFE.

Results and Analysis

Several polymer films were prepared with different TrFE proportions ranging from 20% up to 79%. These films were fabricated by drop-casting 15 wt.% polymer solutions on glass substrates and subsequently drying the films on a hotplate for 2h 20 min at a temperature of 90 °C (atmospheric pressure). No post-processing thermal annealing steps were applied to these films, allowing the polymer to slowly crystallize with solvent

evaporation. No shearing forces were applied during deposition. All the used copolymers presented similar molecular weights (*ca.* 2×10^5 kg mol^{-1}, see SI). Therefore, the molecular weight of these copolymers is also not expected to introduce sample variability, and the observed changes are related to their composition. The prepared films were detached from the glass substrate by immersion in deionized water to obtain free-standing films for characterization. A combination of SAXS and AFM (with additional SEM support – SI) was used to study the evolution of the polymer crystallites (morphology, size, and structure) as the TrFE content increased. We begin by discussing the structural features observed and extracted from the SAXS patterns.

SAXS Analysis:

SAXS measurements were performed on free-standing polymer films, with the film surface perpendicular to the X-ray beam. The 2D diffraction patterns were recorded over a q range from 0.004 to 0.17 Å^{-1}, followed by azimuthal pattern integration to obtain 1D distribution functions (shown in the SI, Figure S1). The Lorentz corrected patterns are plotted in Fig. 1a. The patterns were fitted with several Gaussian profiles, labelled G1 to G3. Three Gaussian profiles could be resolved for samples with TrFE proportions up to 50%, after which only two profiles were properly resolved. The intensity of the G3 profile decreases with increasing TrFE content while also increasing profile breadth. This suggests that the structural features that result in the G3 Gaussian distribution gradually vanish as the TrFE content increases. The sum of the different Gaussian profiles results in the Cumulative fit function (shown in greater detail in the SI). The cumulative fit and the individual Gaussian distributions can be employed in the calculation of the correlation functions, $K(z)$, which provides additional information on the spatial periods of these distributions.[28–33] The calculation of the different $K(z)$ functions is thoroughly discussed in the SI. The calculated $K(z)$ for the cumulative and Gaussian profiles are plotted in Figs. 1b and 1c, respectively, and normalized to their respective $K(0)$. The cumulative $K(z)$ functions (Fig. 1b) show a complex oscillation pattern with different local maxima due to the presence of different distributions. The first absolute maxima for $z > 0$ correspond to the long period of the cumulative distribution. In this case, the maxima correspond to the long period of the G1 distributions. A shift in the calculated cumulative $K(z)$ is also observed (black arrow), increasing the distribution long period with TrFE,

up to a content of 50%. The calculated $K(z)$ for each Gaussian profile, plotted in Fig. 1c, are better suited for the determination of the spatial periodicities of the different distributions, in particular the long periods, L, and the size of the crystalline (or high density) domains, d_c. L and d_c are related to the periodic distribution of the material, which can be represented in 1 D by a periodic layered/lamellar structure, as depicted in Fig. 1d. It is this modulation in material (electron) density (high- and low-density regions) that yields a scattering distribution profile in the SAXS data. For the case of semi-crystalline polymers, these distributions are represented by slabs of crystalline regions (high density) periodically intercalated by amorphous regions (low density).[30–32] The long periods, L, correspond to the z-values that result in the first local maximum of $K(z)$, for $z > 0$; while d_c is obtained by determining the value of z of the interception between two linear functions: the minimum of $K(z)$ and the linear regression of the first monotonic decrease of $K(z)$. A detailed description of this method is available in the SI. This analysis was performed for the G1 and G2 Gaussian distributions. The G3 distributions are considerably broader, hindering the proper determination of the long periods (for TrFE contents of 25% to 50%, the $K(z)$ functions become practically flat after the first minimum). These values are plotted in Fig. 1e, for the G1 (L_1 and d_c^1) and G2 (L_2 and d_c^2) distributions. The different periods (L_1, L_2, d_c^1, and d_c^2) have a downward parabola trend with the TrFE content, gradually increasing until reaching maxima at 50% TrFE. After this, all variables decrease with the TrFE content, although not at the same rate. The relative increase of L_1 and L_2 (normalized to the L_1 and L_2 values for 20% TrFE) was also calculated and is plotted in Fig. 1f. This plot clearly shows that these two quantities decrease at different rates for TrFE contents above 50% despite presenting maxima at 50%. At 79% TrFE the G1 distribution presents a L_1 value around 26% higher than that determined for 20% TrFE, while the G2 distribution returns to L_2 values around those for 20% TrFE. L_1 and L_2 present maxima at 50% TrFE of the order of 40% and 30%, respectively. To understand the type of structures that result in the observed Gaussian distributions (stacks, lamella, or other periodic features), several AFM scans were performed in PeakForce mode. These are discussed in the next section.

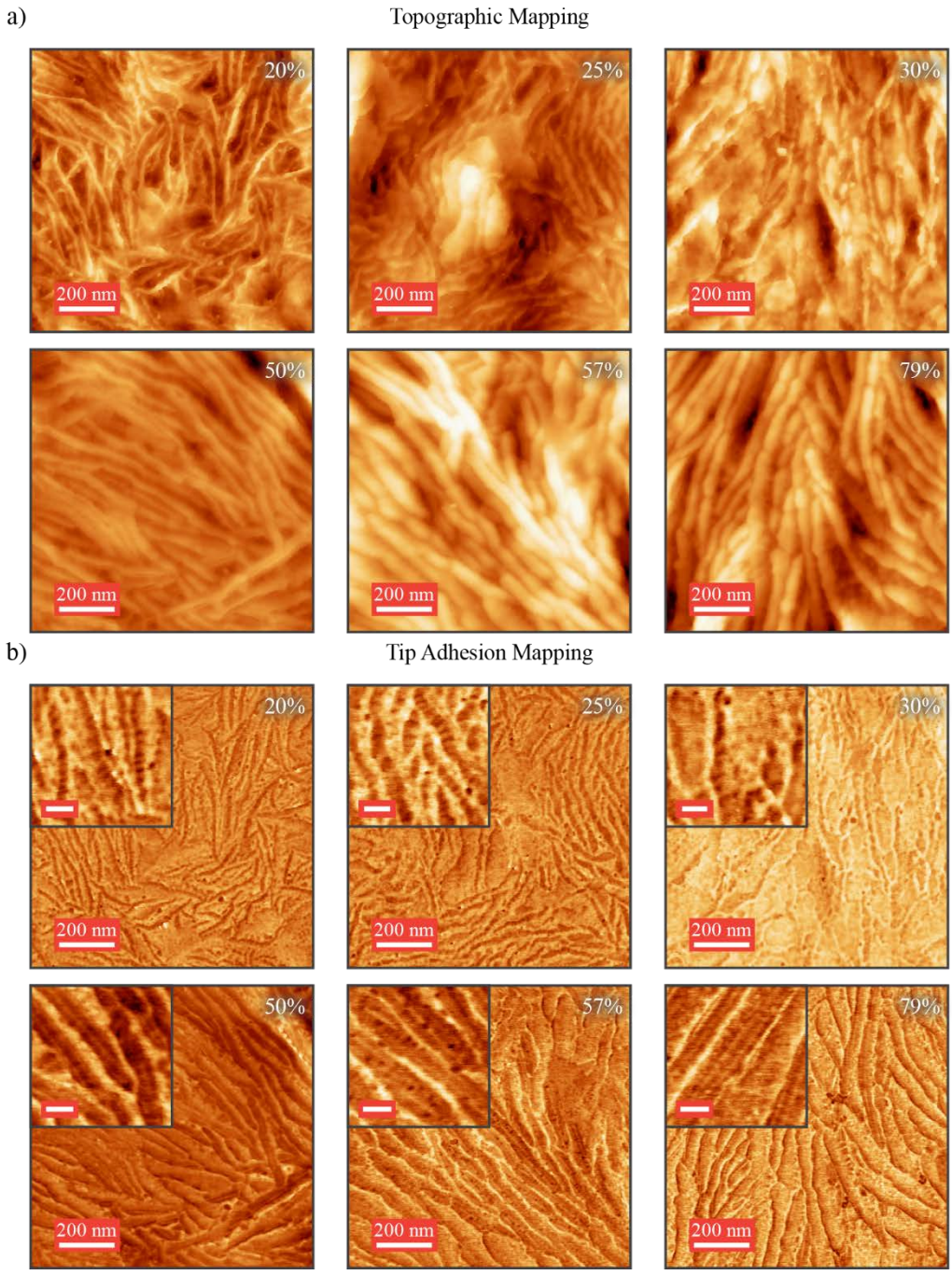

Figure 2. AFM characterization. a) AFM topography scans. b) AFM tip adhesion mapping through AFM PeakForce QNM scans showing additional structural features within the long fiber and rod-like (stacks) domains. The insets are close-up of the same scans showing additional structural features composed of periodic ridges and planes (inner-stack features). Scale bar: 40 nm.

Morphology features deduced from AFM:

The morphology of the copolymer films was analyzed with AFM. AFM topographic scans are displayed in Fig. 2a. The AFM results reveal a clear evolution in film morphology as a function of the TrFE content. The crystalline domains exhibit a rod or fiber-like morphology, which grow in both thickness and length as the TrFE content increases. The smallest features were observed for 20% TrFE. A closer examination indicated changes in domain orientation, where most crystalline domains displayed an edge-on orientation relative to the substrate. However, several flat-on domains were also noted, particularly in samples with 25% and 30% TrFE. The appearance of these flat-on domains suggests that the polymer crystalline domains possess a discoid shape, manifesting as rod-like structures in edge-on orientations. For higher proportions of TrFE (57% and 79%), these domains appeared to orient at an intermediate angle between fully edge-on and flat-on, resulting in step-like regions composed from the stacking of multiple discoid-shaped domains. The morphology, size, and orientation of these domains were further corroborated through SEM imaging (see SI, Fig. S5). The SEM observations confirmed the trend in domain orientation: predominantly edge-on domains were found in samples with less than 50% TrFE, while stacked angled domains forming step-like regions were characteristic of samples with TrFE content exceeding 50%. The orientation of the crystalline domains is an important factor that influences the magnitude of the electroactive response of these materials. When an external electric field is applied, only the dipoles with parallel rotation planes to the electric field will align in the direction of the field. This is the case of crystalline domains that orient edge-on with respect to the substrate, having the crystallographic *b*-axis perpendicular to the substrate. The presence of flat-on domains further decreases the electric responsiveness of the material.[15,27] Because of this behavior, it becomes important to understand how these domains orient under different processing and composition.

Additional information on the structure of the crystalline domains were obtained from the AFM tip adhesion mapping related to the sample mechanical response *via* the tip-sample interaction. As amorphous and crystalline regions have distinct mechanical properties and densities, a mapping of these structural features can be obtained. The different scans (performed simultaneously to the topographic scans) are shown in Fig. 2b. The insets correspond to close-ups from the same scans, to better visualize the detected small variations

in mechanical adhesion. This approach also eliminates the effects of large topographic variations. The adhesion images show important nanometric features (inner-stack features) inside the crystalline domains (stack) of the polymer. In particular, the different copolymers seemed to present hierarchical arrangement of their crystalline domains (stacks). For TrFE proportions below 50%, the stacks displayed periodic ridges with elliptical shapes, whereas at 50% and above, the stacks transitioned to long lamellar structures. Accordingly, these scans indicate that the crystalline domains of the polymers not only show a certain degree of hierarchical arrangement but also change the morphology of this arrangement depending on the TrFE content. The average thickness of these features (stack and inner-stack) was directly retrieved from these scans and is shown in Fig. 3a. The thickness of the polymer stacks appears to increase monotonically with increasing TrFE content, which contrasts with the trend observed in the SAXS data. However, as mentioned above, the orientation of the stacks was also observed to change for high TrFE proportions, presenting an intermediate angle with the substrate which will increase the projected thickness (illustration shown on the plot). The thickness values for low TrFE proportions and the average thicknesses of the inner-stack features correspond well with d_c^1 and d_c^2 values extracted from the SAXS measurements (also plotted, diamonds). This result suggests that the Gaussian distributions G1 and G2 derived from the SAXS analysis likely correspond to polymer stacks and the inner polymer crystalline ridges/lamellae, respectively. An illustration of this hierarchical arrangement is shown in Fig. 3b, showing that the copolymer crystalline structures display an orthogonal hierarchical arrangement (periodic ridges within a long stack) for TrFE proportions below 50%, and a parallel hierarchical arrangement (lamellae within a stack) for 50% TrFE and above. Considering the elliptical morphology of the ridges for low TrFE content, it is plausible that the third Gaussian distribution, G3, is associated with the small axis of the elliptical structures. The disappearance of the G3 distribution for proportions above 50% is also consistent with the observed change in structural features. However, from the recorded data it is unclear what type of structure exists within the polymer stacks that gives origin to these elliptical distributions observed for edge-on domains. Given that the SAXS experimental conditions probe two out of the three-dimensional axis, these elliptical structures are likely originated from a 3D organization of the polymer crystalline domains inside the stacks and not a surface effect that occurs on the stack edge.

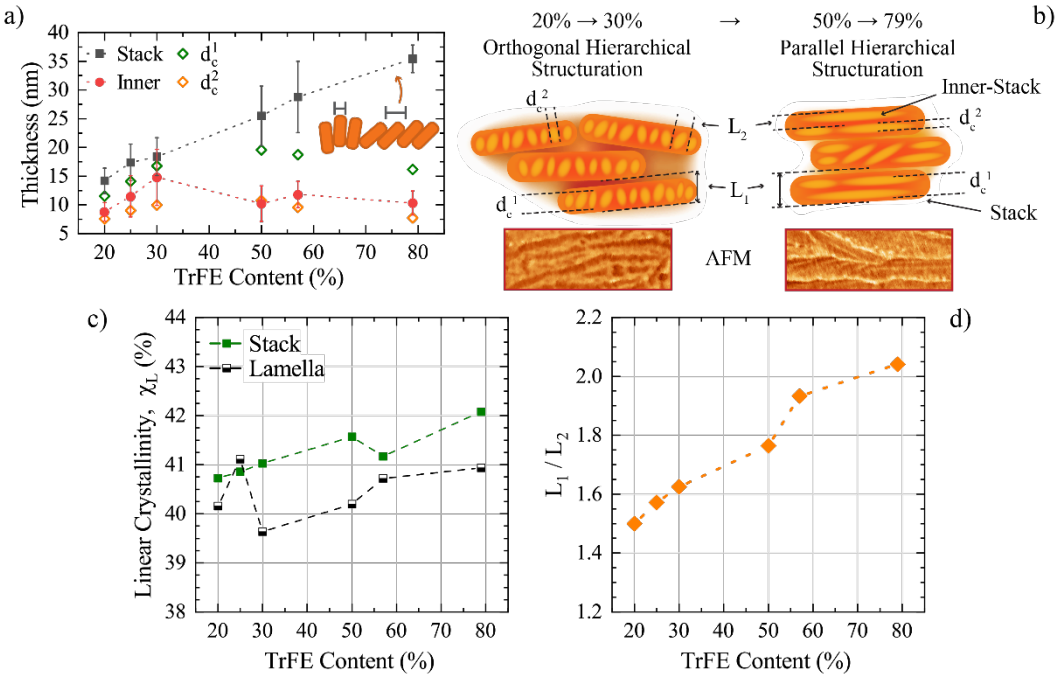

Figure 3. Polymer stack thickness and structure, linear crystallinity, and long-period ratio. a) Thickness of the stack and inter-stack features as measured from the AFM scans and compared to the obtained d_c values from the SAXS correlation functions. b) Scheme of the observed morphological features, and evolution from periodic orthogonal ridges to parallel laminar features. c) Linear crystallinity calculated for the stacks and lamellae (G1 and G2 profiles, see SI) *vs.* TrFE content. d) Ratio of the stack long period (L_1) and the lamellae long period (L_2), showing an increase in the number of lamellar structures inside the polymer stacks as the TrFE content increases.

Discussion

The combined insights from X-ray structural characterization and AFM morphological analysis allowed the identification of distinct morphological features corresponding to the different Gaussian distributions observed in the SAXS patterns. This analysis sheds light on the structural evolution of the copolymers with increasing TrFE content. From the SAXS long periods, we can further extract the linear (1D) crystallinity χ_L (see SI) of the polymer stacks and lamellae, plotted in Fig. 3c. χ_L is given by the ratio between the crystalline domain, d_c, and the total periodic domain, L. For both the polymer stacks and lamellae, χ_L increases with increasing TrFE content, although the overall changes are relatively small, with absolute increases slightly above 1%. Interestingly, despite a decrease in all spatial periodicities observed beyond 50% TrFE, χ_L continues to increase. This suggests that local crystallinity appears to slowly increase with TrFE content. χ_L is expected to

be larger than the actual polymer crystallinity (volumetric) as χ_L does not consider large scattered amorphous domains (such as amorphous inclusions, amorphous grain/spherulite boundaries, *etc.*). The small difference in χ_L between the stacks and lamellae, around 1%, suggests that the proportion of crystalline material within these structures is similar. It is relevant to mention that lamellar structures are typically contained within polymer stacks, but the periodic spacing and the ratio of amorphous to crystalline domains can differ. An exception is observed for the lamellar χ_L, where the sample with 25% TrFE exhibits a higher linear crystallinity. In a previous study, we have analyzed P(VDF-TrFE) copolymers ranging up to 50% TrFE and noted an abnormal increase in the Curie transition enthalpy on calorimetric data (DSC).[7] We attributed this increase to a more cohesive crystalline phase, which enhances dipolar interactions within these ferroelectric materials, potentially increasing the transition enthalpy. The sudden increase in linear crystallinity supports this hypothesis, suggesting a higher local degree of order at the lamellar level, which favours dipolar cooperation.

The SAXS and AFM data have revealed an evolution of the thickness and length of the stack and lamellar structures with the amount of TrFE. The long periods and the size of the crystalline domains (L and d_c) followed a downward parabola-like trend with maxima at 50% TrFE (Fig. 1). This trend suggests an expansion of the stack/lamellar structures, reaching a maximum around 50% TrFE. As the calculated χ_L only presents a small monotonic increase with TrFE, we can also conclude that the expansion of these domains does not play a significant role on polymer crystallinity and should be related primarily to conformational changes at the polymer chain level. Indeed, conformational changes have been reported for this range of TrFE contents (from 45% to 55%) related to the presence of a morphotropic phase boundary that reflects a transition from ferroelectric to relaxor-ferroelectric behavior in these copolymers.[6,22,34,35] The increase in *trans-gauche* defects along the polymer chain introduces conformational defects that form kinks along the polymer backbone, potentially expanding the inter-chain volume without significant changes of the local crystallinity. This hypothesis agrees well with recent literature on P(VDF-TrFE) copolymers, explaining the observed trends with TrFE content.[6,7,22,34,35]

Lastly, the ratio between the long periods of the stacks (L_1) and the lamellae (L_2) was also calculated and is plotted on Fig. 3d. We have seen that L_1 and L_2 follow a similar trend with TrFE, but that L_2 decreased much faster after its maximum at 50% TrFE. Their ratio shows that the proportion of lamellae per stack increases with TrFE, with each stack containing on average 2 lamellae for high TrFE content, in contrast to *ca.* 1.5 lamellae per stack at low TrFE contents. The analysis points to an overall increase in local crystallinity (χ_L) as well as a more compact morphology (higher number of lamellae per stack) with increasing TrFE contents.

Conclusion

In this work, we have analyzed the structural and morphological features of different P(VDF-TrFE) copolymers with varying TrFE content, ranging from 20% up to 79%. The analysis of the SAXS profiles and the corresponding correlation functions revealed the presence of multiple structural distributions (three distinct Gaussian distributions – G1, G2, and G3), each characterized by different long periods and sizes of the crystalline domains (labelled L and d_c respectively). These change with the TrFE proportion following a downward parabola-like trend with maxima at 50% TrFE, which we have associated to an expansion of the stack/lamellar structures. This expansion likely arises from an increase in the inter-chain volume due to the formation of conformational defects along the chain backbone. These maxima coincide with the reported compositional range for which the P(VDF-TrFE) morphotropic phase boundary takes place. The rates of decrease were also observed to be different, with the second Gaussian distribution (G2, with L_2 and d_c^2) decreasing much faster than the first Gaussian distribution (G1, with L_1 and d_c^1). The AFM characterization further elucidated the morphology of the polymer crystallites, revealing a certain degree of hierarchical arrangement. The stack-like features were associated with the largest detected periods of G1 (L_1 and d_c^1), while the inner-stack modulations corresponded to crystalline lamellae associated with the G2 distribution (L_2 and d_c^2). The type of structural organization was observed to shift from ridge-like periodic undulations (for TrFE up to 50%) to the typical stacked lamellae (from 50% upwards) usually found in these systems. Lastly, the linear crystallinity and the ratio of Lamella to Stack was evaluated. A monotonic increase in linear crystallinity with increasing TrFE content was observed, suggesting that higher TrFE levels promote higher

local crystallinity. The lamella to stack ratio also increased monotonically with TrFE content, indicating that despite a decrease in the spatial periodicity of all structures, the number of lamellae per stack continued to increase, reaching a maximum of 2 lamellae per stack at 79% TrFE, compared to 1.5 lamellae per stack at 20% TrFE.

Supporting Information

Corresponding Author

Pedro M. Resende - Université de Bordeaux, CNRS, Bordeaux INP, LCPO, UMR 5629, F-33600, Pessac, France. ORCiD: orcid.org/0000-0001-7854-2297. Email: pdecamposres@u-bordeaux.fr

Guillaume Fleury - Université de Bordeaux, CNRS, Bordeaux INP, LCPO, UMR 5629, F-33600, Pessac, France. ORCiD: orcid.org/0000-0003-0779-191X. Email: gfleury@enscbp.fr

Authors

Sara Zanchi - Université de Bordeaux, CNRS, Bordeaux INP, LCPO, UMR 5629, F-33600, Pessac, France.

Jean-David Isasa - Université de Bordeaux, CNRS, Bordeaux INP, LCPO, UMR 5629, F-33600, Pessac, France.

Raymond Khayat - Université de Bordeaux, CNRS, Bordeaux INP, LCPO, UMR 5629, F-33600, Pessac, France.

Georges Hadziioannou - Université de Bordeaux, CNRS, Bordeaux INP, LCPO, UMR 5629, F-33600, Pessac, France. ORCiD: orcid.org/0000-0002-7377-6040

Conflicts of Interest

The authors declare no conflicts of interest.

Acknowledgements

The authors acknowledge the financial support from the Industrial Chair SMILE within the Grant Agreement No. ANR-19-CHIN-0002. The authors thank Arkema-Piezotech (France) for providing the materials used in the study.

References

(1) Li, H.; Wang, R.; Han, S.-T.; Zhou, Y. Ferroelectric Polymers for Non-Volatile Memory Devices: A Review. *Polymer International* **2020**, *69* (6), 533–544. https://doi.org/10.1002/pi.5980.
(2) Thuau, D.; Kallitsis, K.; Santos, F. D. D.; Hadziioannou, G. All Inkjet-Printed Piezoelectric Electronic Devices: Energy Generators, Sensors and Actuators. *Journal of Materials Chemistry C* **2017**, *5* (38), 9963–9966. https://doi.org/10.1039/C7TC02558K.
(3) Chen, X.; Han, X.; Shen, Q.-D. PVDF-Based Ferroelectric Polymers in Modern Flexible Electronics. *Advanced Electronic Materials* **2017**, *3* (5), 1600460. https://doi.org/10.1002/aelm.201600460.
(4) Aliane, A.; Benwadih, M.; Bouthinon, B.; Coppard, R.; Domingues-Dos Santos, F.; Daami, A. Impact of Crystallization on Ferro-, Piezo- and Pyro-Electric Characteristics in Thin Film P(VDF–TrFE). *Organic Electronics* **2015**, *25*, 92–98. https://doi.org/10.1016/j.orgel.2015.06.007.
(5) Bargain, F.; Panine, P.; Domingues Dos Santos, F.; Tencé-Girault, S. From Solvent-Cast to Annealed and Poled Poly(VDF-Co-TrFE) Films: New Insights on the Defective Ferroelectric Phase. *Polymer* **2016**, *105*, 144–156. https://doi.org/10.1016/j.polymer.2016.10.010.
(6) Liu, Y.; Zhang, B.; Xu, W.; Haibibu, A.; Han, Z.; Lu, W.; Bernholc, J.; Wang, Q. Chirality-Induced Relaxor Properties in Ferroelectric Polymers. *Nat. Mater.* **2020**, *19* (11), 1169–1174. https://doi.org/10.1038/s41563-020-0724-6.
(7) Resende, P. M.; Isasa, J.-D.; Hadziioannou, G.; Fleury, G. Deciphering TrFE Fingerprints in P(VDF-TrFE) by Raman Spectroscopy: Defect Quantification and Morphotropic Phase Boundary. *Macromolecules* **2023**, *56* (23), 9673–9684. https://doi.org/10.1021/acs.macromol.3c01700.
(8) Bargain, F.; Thuau, D.; Panine, P.; Hadziioannou, G.; Domingues Dos Santos, F.; Tencé-Girault, S. Thermal Behavior of Poly(VDF-Ter-TrFE-Ter-CTFE) Copolymers: Influence of CTFE Termonomer on the Crystal-Crystal Transitions. *Polymer* **2019**, *161*, 64–77. https://doi.org/10.1016/j.polymer.2018.11.064.
(9) Lovinger, A. J.; Davis, D. D.; Cais, R. E.; Kometani, J. M. Compositional Variation of the Structure and Solid-State Transformations of Vinylidene Fluoride/Tetrafluoroethylene Copolymers. *Macromolecules* **1988**, *21* (1), 78–83. https://doi.org/10.1021/ma00179a017.
(10) Tashiro, K.; Kobayashi, M. Structural Phase Transition in Ferroelectric Fluorine Polymers: X-Ray Diffraction and Infrared/Raman Spectroscopic Study. *Phase Transitions: A Multinational Journal* **1989**. https://doi.org/10.1080/01411598908206864.
(11) Furukawa, T. Ferroelectric Properties of Vinylidene Fluoride Copolymers. *Phase Transitions* **1989**, *18* (3–4), 143–211. https://doi.org/10.1080/01411598908206863.
(12) Bourgaux-Leonard, C.; Legrand, J. F.; Renault, A.; Delzenne, P. Annealing Effects in Ferroelectric Poly(Vinylidene Fluoride-Trifluoroethylene) Copolymers: Real-Time Studies Using Synchrotron Radiation. *Polymer* **1991**, *32* (4), 597–604. https://doi.org/10.1016/0032-3861(91)90470-4.
(13) Hu, J.; Zhang, J.; Fu, Z.; Jiang, Y.; Ding, S.; Zhu, G. Solvent Vapor Annealing of Ferroelectric P(VDF-TrFE) Thin Films. *ACS Appl. Mater. Interfaces* **2014**, *6* (20), 18312–18318. https://doi.org/10.1021/am5055299.

(14) Spampinato, N.; Maiz, J.; Portale, G.; Maglione, M.; Hadziioannou, G.; Pavlopoulou, E. Enhancing the Ferroelectric Performance of P(VDF-Co-TrFE) through Modulation of Crystallinity and Polymorphism. *Polymer* **2018**, *149*, 66–72. https://doi.org/10.1016/j.polymer.2018.06.072.
(15) Zanchi, S.; Pascaud, A.; Domingues Dos Santos, F.; Tencé-Girault, S.; Roland, S. Nanometric and Macroscopic Electroactive Response of P(VDF-Co-TrFE) Copolymers and P(VDF-Ter-TrFE-Ter-CTFE) Terpolymers. *ACS Appl. Polym. Mater.* **2023**, *5* (7), 4966–4976. https://doi.org/10.1021/acsapm.3c00534.
(16) Xie, K.; Housseini, J.; Resende, P. M.; Le Goupil, F.; Isasa, J.; Tencé-Girault, S.; Fleury, G.; Kellay, H.; Hadziioannou, G. Enhanced Pyroelectricity Over Extended Thermal Range in Flexible Polymer Thin Films. *Adv Funct Materials* **2024**, 2411397. https://doi.org/10.1002/adfm.202411397.
(17) Choi, S. T.; Kwon, J. O.; Bauer, F. Multilayered Relaxor Ferroelectric Polymer Actuators for Low-Voltage Operation Fabricated with an Adhesion-Mediated Film Transfer Technique. *Sensors and Actuators A: Physical* **2013**, *203*, 282–290. https://doi.org/10.1016/j.sna.2013.08.049.
(18) Jiang, H.; Yang, J.; Xu, F.; Wang, Q.; Liu, W.; Chen, Q.; Wang, C.; Zhang, X.; Zhu, G. VDF-Content-Guided Selection of Piezoelectric P(VDF-TrFE) Films in Sensing and Energy Harvesting Applications. *Energy Conversion and Management* **2020**, *211*, 112771. https://doi.org/10.1016/j.enconman.2020.112771.
(19) Li, W.; Zhu, Y.; Hua, D.; Wang, P.; Chen, X.; Shen, J. Crystalline Morphologies of P(VDF-TrFE) (70/30) Copolymer Films above Melting Point. *Applied Surface Science* **2008**, *254* (22), 7321–7325. https://doi.org/10.1016/j.apsusc.2008.05.339.
(20) Lee, J. S.; Prabu, A. A.; Kim, K. J. Annealing Effect upon Chain Orientation, Crystalline Morphology, and Polarizability of Ultra-Thin P(VDF-TrFE) Film for Nonvolatile Polymer Memory Device. *Polymer* **2010**, *51* (26), 6319–6333. https://doi.org/10.1016/j.polymer.2010.10.053.
(21) Guo, D.; Stolichnov, I.; Setter, N. Thermally Induced Cooperative Molecular Reorientation and Nanoscale Polarization Switching Behaviors of Ultrathin Poly(Vinylidene Fluoride-Trifluoroethylene) Films. *J. Phys. Chem. B* **2011**, *115* (46), 13455–13466. https://doi.org/10.1021/jp2061442.
(22) Hafner, J.; Benaglia, S.; Richheimer, F.; Teuschel, M.; Maier, F. J.; Werner, A.; Wood, S.; Platz, D.; Schneider, M.; Hradil, K.; Castro, F. A.; Garcia, R.; Schmid, U. Multi-Scale Characterisation of a Ferroelectric Polymer Reveals the Emergence of a Morphological Phase Transition Driven by Temperature. *Nat Commun* **2021**, *12* (1), 152. https://doi.org/10.1038/s41467-020-20407-6.
(23) Disnan, D.; Hafner, J.; Schneider, M.; Schmid, U. Spherulite-like Microstructure Observed for Spin-Cast P(VDF-TrFE) Thin Films and Their Ferroelectric Characteristics. *Polymer* **2023**, 125840. https://doi.org/10.1016/j.polymer.2023.125840.
(24) Zanchi, S.; Engel, M.; Pascaud, A.; Bargain, F.; Lebreton, S.; Domingues dos Santos, F.; Roland, S.; Tencé-Girault, S. Unraveling the Morphological Diversity of P(VDF-Ter-TrFE-Ter-CTFE) Semi-Crystalline Terpolymers via Combined AFM and SAXS Experiments. *Polymer Testing* **2023**, *120*, 107973. https://doi.org/10.1016/j.polymertesting.2023.107973.
(25) Hirose, R.; Yoshioka, T.; Yamamoto, H.; Reddy, K. R.; Tahara, D.; Hamada, K.; Tashiro, K. In-House Simultaneous Collection of Small-Angle X-Ray Scattering, Wide-Angle X-Ray Diffraction and Raman Scattering Data from Polymeric Materials. *Journal of Applied Crystallography* **2014**, *47* (3), 922–930. https://doi.org/10.1107/S1600576714006724.
(26) Tashiro, K.; Tanaka, R. Structural Correlation between Crystal Lattice and Lamellar Morphology in the Ferroelectric Phase Transition of Vinylidene Fluoride–Trifluoroethylene Copolymers as Revealed by the Simultaneous Measurements of Wide-Angle and Small-Angle X-Ray Scatterings. *Polymer* **2006**, *47* (15), 5433–5444. https://doi.org/10.1016/j.polymer.2005.06.128.
(27) Kim, J.-H.; Khang, D.-Y. High-Performance Needle-Shaped Crystals in Thin and Ultrathin P(VDF-TrFE) Films Formed by Melt Recrystallization. *European Polymer Journal* **2014**, *59*, 78–83. https://doi.org/10.1016/j.eurpolymj.2014.07.017.
(28) Strobl, G. R.; Schneider, M. Direct Evaluation of the Electron Density Correlation Function of Partially Crystalline Polymers. *Journal of Polymer Science: Polymer Physics Edition* **1980**, *18* (6), 1343–1359. https://doi.org/10.1002/pol.1980.180180614.
(29) Buckley, J.; Cebe, P.; Cherdack, D.; Crawford, J.; Ince, B. S.; Jenkins, M.; Pan, J.; Reveley, M.; Washington, N.; Wolchover, N. Nanocomposites of Poly(Vinylidene Fluoride) with Organically Modified Silicate. *Polymer* **2006**, *47* (7), 2411–2422. https://doi.org/10.1016/j.polymer.2006.02.012.
(30) Goderis, B.; Reynaers, H.; Koch, M. H. J.; Mathot, V. B. F. Use of SAXS and Linear Correlation Functions for the Determination of the Crystallinity and Morphology of Semi-Crystalline Polymers. Application to Linear Polyethylene. *Journal of Polymer Science Part B: Polymer Physics* **1999**, *37* (14), 1715–1738. https://doi.org/10.1002/(SICI)1099-0488(19990715)37:14<1715::AID-POLB15>3.0.CO;2-F.

(31) Basiura-Cembala, M.; Erlacher, K.; Pedersen, J. S.; Goderis, B. Phase Densities and Lamellar Morphologies of Semicrystalline Polyethylenes via Absolute Small-Angle X-Ray Scattering Measurements. *Journal of Applied Crystallography* **2015**, *48* (5), 1498–1506. https://doi.org/10.1107/S1600576715014752.
(32) Seidlitz, A.; Thurn-Albrecht, T. Small-Angle X-Ray Scattering for Morphological Analysis of Semicrystalline Polymers. In *Polymer Morphology*; John Wiley & Sons, Ltd, 2016; pp 151–164. https://doi.org/10.1002/9781118892756.ch9.
(33) Rozanski, A.; Safandowska, M.; Krajenta, A. DSC/SAXS Analysis of the Thickness of Lamellae of Semicrystalline Polymers-Restrictions in the Case of Materials with Swollen Amorphous Phase. *Polymer Testing* **2018**, *65*, 189–196. https://doi.org/10.1016/j.polymertesting.2017.11.028.
(34) Liu, Y.; Aziguli, H.; Zhang, B.; Xu, W.; Lu, W.; Bernholc, J.; Wang, Q. Ferroelectric Polymers Exhibiting Behaviour Reminiscent of a Morphotropic Phase Boundary. *Nature* **2018**, *562* (7725), 96–100. https://doi.org/10.1038/s41586-018-0550-z.
(35) Liu, Y.; Chen, X.; Han, Z.; Zhou, H.; Wang, Q. Defects in Poly(Vinylidene Fluoride)-Based Ferroelectric Polymers from a Molecular Perspective. *Applied Physics Reviews* **2022**, *9* (3), 031306. https://doi.org/10.1063/5.0097446.